

# Improving Parameterization of Rain Microphysics with Disdrometer and Radar Observations

GUIFU ZHANG

*School of Meteorology, University of Oklahoma, Norman, Oklahoma*

JUANZHEN SUN AND EDWARD A. BRANDES

*National Center for Atmospheric Research, Boulder, Colorado*

(Manuscript received 16 March 2005, in final form 6 September 2005)

## ABSTRACT

Disdrometer observations indicate that the raindrop size distribution (DSD) can be represented by a constrained-gamma (CG) distribution model. The model is used to retrieve DSDs from polarization radar measurements of reflectivity and differential reflectivity and to characterize rain microphysics and physical processes such as evaporation, accretion, and precipitation. The CG model parameterization is simplified to a single parameter for application in single-moment numerical models. This simplified parameterization is applied in the Variational Doppler Radar Analysis System (VDRAS) using Kessler-type parameterizations for model initialization and forecasting. Results are compared to those for the Marshall–Palmer (MP) DSD model. It is found that the simplified CG model parameterization better preserves the stratiform rain and produces better forecasts than the MP model parameterization.

## 1. Introduction

Understanding and characterization of precipitation microphysics is needed for improving parameterization in numerical weather prediction (NWP) models (Droegemeier et al. 2000; Sun 2005; Zhao and Carr 1997). Early, microphysical parameterizations were mostly single-moment (bulk water) schemes (Kessler 1969). Recently, two-moment parameterization schemes and spectral models have received attention (e.g., Ferrier 1994; Meyers et al. 1997; Hong et al. 2004; Chen and Liu 2004). In addition to rainwater mixing ratio, two-moment models typically forecast total drop concentration and diagnose the mean particle diameter. Spectral models start with a stochastic collection equation and solve for the temporal and spatial changes in the drop spectra. While two-moment parameterizations provide additional freedom in describing microphysics and spectral models are more rigorous, single-moment

parameterization is still widely used (Walko et al. 1995; Thompson et al. 2004), for example, in the fifth-generation Pennsylvania State–National Center for Atmospheric Research (PSU–NCAR) Mesoscale Model (MM5) and Weather Research and Forecast (WRF) models, because of its simplicity and computational efficiency.

The fundamental characterization of rain microphysics is through the raindrop size distribution (DSD). Microphysical processes of evaporation, accretion, and precipitation rate are all related by the DSD. The parameterization scheme of Kessler (1969) was developed on the assumption of an exponential distribution of raindrops, written as

$$N(D) = N_0 \exp(-\Lambda D), \quad (1)$$

where the slope parameter  $\Lambda$  relates to a characteristic size of the raindrops such as the mean diameter [ $\langle D \rangle = (2/\Lambda)$ ] or median volume diameter [ $D_0 \approx (3.67/\Lambda)$ ]. Here,  $N_0$  is an intercept parameter, which was fixed at  $10\,000 \text{ m}^{-3} \text{ mm}^{-1}$  by Kessler. When  $N_0 = 8000 \text{ m}^{-3} \text{ mm}^{-1}$ , Eq. (1) becomes the Marshall–Palmer (MP) drop size distribution (Marshall and Palmer 1948). For

---

*Corresponding author address:* Dr. Guifu Zhang, School of Meteorology, University of Oklahoma, 100 E. Boyd Street, Norman, OK 73019.  
E-mail: guzhang1@ou.edu

the MP DSD model and Kessler's parameterization scheme, microphysical processes for evaporation rate ( $R_e$  in  $\text{g m}^{-3} \text{s}^{-1}$ ) for a unit water vapor saturation deficit, accretion rate ( $R_c$  in  $\text{g m}^{-3} \text{s}^{-1}$ ) for a unit cloud water content, and mass-weighted terminal velocity ( $V_{tm}$  in  $\text{m s}^{-1}$ ) can be represented in terms of rainwater content ( $W$  in  $\text{g m}^{-3}$ ) as follows:

$$R_e = 5.03 \times 10^{-4} W^{13/20} \quad (2)$$

$$R_c = 5.08 \times 10^{-3} W^{7/8} \quad (3)$$

$$V_{tm} = 5.32 W^{1/8}. \quad (4)$$

The radar reflectivity factor at horizontal polarization ( $Z_H$  in  $\text{mm}^6 \text{m}^{-3}$ ) is related to water content by

$$Z_H = 2.04 \times 10^4 W^{7/4}. \quad (5)$$

Although there have been some modifications, for example, by Miller and Pearce (1974), Clark (1977), Klemp and Wilhelmson (1978), Lin et al. (1983), and Rutledge and Hobbs (1983), this simple approach to model parameterization, called a Kessler-type scheme, is still widely used in mesoscale models. As noted by Kessler (1969, p. 30), an exponential DSD model with a fixed intercept "does some violence to the physics of the evaporation process". The problem with fixed-intercept parameterizations is that the rainwater gets redistributed into smaller drop categories as the drop spectra slope parameter increases, thus accelerating the process of rainwater removal through evaporation. Rainfall rate cannot be accurately estimated with an  $R$ - $Z$  relation derived from the MP DSD model (Wilson and Brandes 1979, their Table 3). The uncertainty of rain-rate estimation can be as high as 50% (Smith et al. 1975, 1993; Hagen and Yuter 2003). The coefficients and exponents in (2)–(5) are often arbitrarily adjusted to improve forecast results (Miller and Pearce 1974; Sun and Crook 1997). However, such adjustments are mostly empirical (Liu and Daum 2004) and lack verification with observations. Another problem with the Kessler-type scheme occurs when an adjoint model is derived in a four-dimensional data assimilation (4DVAR) system. Because of the highly nonlinear nature of expressions such as Eqs. (2) and (4), the minimization of the cost function tends to have convergence problems (Sun and Crook 1997).

The gamma distribution has been used to improve the characterization of rain DSDs over the exponential distribution (Ulbrich 1983; Willis 1984). Recent disdrometer observations indicate that rain DSDs can be represented by a constrained-gamma (CG) distribution model (Zhang et al. 2001). The CG model was devel-

oped for retrieving rain DSDs from polarization radar observations. The procedure is to determine the three parameters of the gamma distribution from radar reflectivity, differential reflectivity, and a constraining relation between the shape and slope of the distribution. It has been shown that the CG model characterizes natural DSDs better and leads to more accurate retrievals than that with a two-parameter exponential model and with a variable  $N_0$  (Brandes et al. 2003). The CG rain DSD model allows accurate rainfall estimation and study of storm microphysics through the retrieval of total number concentration, droplet size, and the shape of rain spectra (Brandes et al. 2004a, 2006; Vivekanandan et al. 2004).

In this paper, we apply the constrained-gamma DSD model to the microphysical parameterization in a cloud model and evaluate the impact of the parameterization scheme on the initialization and forecasting of storms. Our ultimate goal is to develop a two-moment scheme that utilizes two polarization radar measurements of  $Z_H$  and  $Z_{DR}$  for model parameterization and initialization. At this moment, however, a two-moment data assimilation system is not available. In addition, the case we studied in this paper does not have volumetric polarization. Therefore, the objective of this manuscript is to (i) show the potential of using polarization radar data for improving model parameterization with the CG model, (ii) simplify it to a single parameter simplified CG model, and (iii) test the simplified CG model in VDRAS for model parameterization and initialization to see the improvements. Section 2 describes the microphysical parameterization based on constrained-gamma DSDs and compares it with the MP distribution model. Section 3 simplifies the CG model parameterization to a single parameter for application in bulk models. Experiments in variational data assimilation and numerical weather prediction are presented in section 4. A summary and discussion are provided in section 5.

## 2. Constrained-gamma DSD model and rain microphysical processes

The constrained-gamma DSD model consists of a gamma distribution in the form (Ulbrich 1983)

$$N(D) = N_0 D^\mu \exp(-\Lambda D) \quad (6)$$

[where  $N_0$  ( $\text{mm}^{-(1-\mu)} \text{m}^{-3}$ ) is a concentration parameter,  $\mu$  is a shape parameter, and  $\Lambda$  ( $\text{mm}^{-1}$ ) is a slope parameter] and a constraining relation between  $\mu$  and  $\Lambda$  given by

$$\Lambda = 0.0365\mu^2 + 0.735\mu + 1.935. \quad (7)$$

Relation (7) was derived from 2D video-disdrometer measurements made in Florida (Zhang et al. 2001) and has been verified by data collected in Oklahoma (Brandes et al. 2003). It has been shown that (7) characterizes natural rain DSD variations quite well and is not purely the result of measurement error (Zhang et al. 2003). It has recently been verified by numerical simulations with a simple rain shaft model (Seifert 2005). The relation applies to both convective and stratiform DSDs except for that at leading edges of convective storms and drizzle rains. Fine tuning for geographical locations/climatology with further observations may improve the model results. Special attention and treatment is required for small drops when  $\mu$  is negative. The negative  $\mu$ s can cause infinite total number concentration and unrealistically large evaporation. Hence,  $\mu$  is forced to  $\mu = -1$  for  $\mu < -1$  and the integration is performed in a finite limit  $[D_{\min}, D_{\max}]$  rather than  $[0, \infty]$ .

The constrained-gamma DSD model represented by (6) and (7) is essentially a two-parameter model much like the exponential distribution or a gamma distribution with a fixed  $\mu$ . The difference, however, is that the constrained-gamma DSD model is capable of describing a variety of drop-size distributions with different spectral shapes: concave upward shape for a broad distribution versus convex for a narrow distribution on a semilogarithm plot. Because  $\mu$  and  $\Lambda$  jointly describe the DSD shape, the characteristic size (e.g., median volume diameter  $D_0$ ) and the spectrum width are related (Brandes et al. 2004b). This makes physical sense because, except at the leading edge of some convective storms, large raindrops are usually accompanied by small drops, which leads to a broad spectrum. On the other hand, small and medium size raindrops are not necessarily accompanied by large drops, for example, stratiform and light convective rain DSDs. A  $\mu - \Lambda$  (or  $\mu - D_0$ ) relation allows better characterization of the raindrop size/spectrum width dependence than a fixed distribution shape without increasing the number of parameters. A fixed  $\mu$  is a special  $\mu - \Lambda$  relation, for example, an exponential distribution ( $\mu = 0$ ).

The  $\mu - \Lambda$  relation facilitates the reliable retrieval of the gamma DSD parameters ( $N_0$ ,  $\mu$ , and  $\Lambda$ ) from polarization radar measurements of radar reflectivity factor ( $Z_H$ ) and differential reflectivity ( $Z_{DR}$ ). Rain physical parameters can then be obtained by integration of the DSD with proper weight. For example, rainwater content ( $W$  in  $\text{g m}^{-3}$ ) is

$$\begin{aligned} W &= \frac{\rho_w \times 10^{-3} \pi}{6} N_0 \int_{D_{\min}}^{D_{\max}} D^{\mu+3} \exp(-\Lambda D) dD \\ &= \frac{\rho_w \times 10^{-3} \pi}{6} N_0 \Lambda^{-(\mu+4)} [\gamma(\Lambda D_{\max}, \mu + 4) \\ &\quad - \gamma(\Lambda D_{\min}, \mu + 4)], \end{aligned} \quad (8)$$

where  $\gamma$  is the incomplete gamma function,  $D_{\min}$  and  $D_{\max}$  are raindrop minimal and maximal diameters. Here,  $D_{\min}$  was set to 0.1 mm;  $D_{\max}$ , the size of the largest drop, can be estimated from radar reflectivity or differential reflectivity (Brandes et al. 2003). For computational convenience, expressions for rainwater content, rainfall rate ( $R$  in  $\text{mm h}^{-1}$ ), total number concentration ( $N_T$  in  $\text{m}^{-3}$ ),  $D_0$  (in mm), and the parameter  $\mu$  can be expressed in terms of  $Z_H$  and  $Z_{DR}$  as (Brandes et al. 2004b)

$$W = 5.589 \times 10^{-4} Z_H \times 10^{(0.223Z_{DR}^2 - 1.124Z_{DR})} \quad (9)$$

$$R = 0.00760 Z_H \times 10^{(0.165Z_{DR}^2 - 0.897Z_{DR})} \quad (10)$$

$$N_T = 2.085 Z_H \times 10^{(0.728Z_{DR}^2 - 2.066Z_{DR})} \quad (11)$$

$$D_0 = 0.171 Z_{DR}^3 - 0.725 Z_{DR}^2 + 1.479 Z_{DR} + 0.717 \quad (12)$$

$$\mu = 6.084 D_0^2 - 29.85 D_0 + 34.64, \quad (13)$$

where  $Z_H$  is in linear units ( $\text{mm}^6 \text{m}^{-3}$ ) and  $Z_{DR}$  is in dB. Relations (9)–(13) have been verified for tropical rain in Florida (Brandes et al. 2003, 2004a,b). The uncertainty for rainwater content estimates is within 10%, similar to that for rainfall rate. The total number concentration estimates are normally within an order of the measurements. The standard error for median volume diameter is less than 0.2 mm. These numbers are for the Florida data and further verifications are needed in other climatological regions. The equations allow detailed study of precipitation microphysics for convective and stratiform precipitation and their evolution (Brandes et al. 2004a). For example, at the same rainfall rate, stratiform rain often has a larger median volume diameter than that for convective rain. Figure 1 shows an example of rain physics retrievals from radar measurements using the CG and MP models. Direct calculations with disdrometer measurements are also presented for reference. The comparison reveals that the MP model (i) overestimates  $N_T$  except for heavy convective rains and has a small dynamic range, (ii) underestimates  $W$  for convective rainfall (1440–1490 UTC),

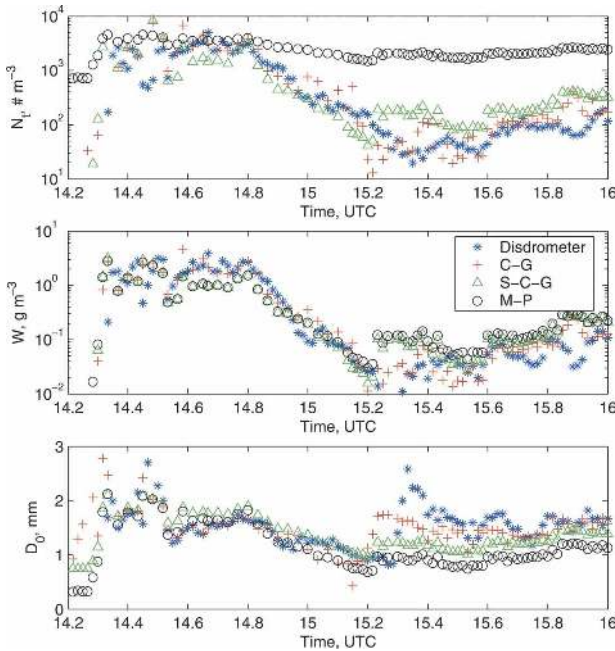


FIG. 1. Time series comparison of estimated total number concentration ( $N_t$ ), rainwater content ( $W$ ), and median volume diameter ( $D_0$ ). Results are shown for disdrometer observations and radar estimates using the CG, SCG, and MP DSD models. Data were collected on 21 Aug 1998 in Florida.

(iii) overestimates  $W$  for stratiform rain (after 1520 UTC), and (iv) underestimates  $D_0$  for stratiform rain. Clearly, the polarization radar-based CG model characterizes rain microphysics more accurately than the reflectivity-based MP model.

Once the rain DSD is known, rain microphysical processes can be estimated. The constrained-gamma DSD model with two independent parameters can be used to derive rain microphysical process parameters: evaporation rate ( $R_e$ ), accretion rate ( $R_c$ ), and mass-weighted terminal velocity ( $V_{tm}$ ). Following Kessler's parameterization procedure, the microphysical process parameters are derived (see appendix) by integration of the gamma DSD (6). Assuming an evaporation coefficient  $E_e = 1$  and accretion coefficient  $E_c = 1$ , we obtain  $R_e$  for a unit vapor saturation deficit ( $m_e = 1 \text{ g m}^{-3}$ ) from (A3),  $R_c$  for a unit cloud water content ( $m_c = 1 \text{ g m}^{-3}$ ) from (A6), and  $V_{tm}$  from (A7), as given by

$$R_e = 6.78 \times 10^{-4} W \Lambda^{7/5} \times \frac{[\gamma(\Lambda D_{\max}, \mu + 13/5) - \gamma(\Lambda D_{\min}, \mu + 13/5)]}{[\gamma(\Lambda D_{\max}, \mu + 4) - \gamma(\Lambda D_{\min}, \mu + 4)]} \quad (14)$$

$$R_c = \frac{3 \times 10^{-3} W}{2} \sum_{i=0}^4 c_i \Lambda^{-i+1} \times \frac{[\lambda(\Lambda D_{\max}, \mu + l + 3) - \gamma(\Lambda D_{\min}, \mu + l + 3)]}{[\gamma(\Lambda D_{\max}, \mu + 4) - \gamma(\Lambda D_{\min}, \mu + 4)]} \quad (15)$$

$$V_{tm} = \sum_{i=0}^4 c_i \Lambda^{-i} \times \frac{[\gamma(\Lambda D_{\max}, \mu + l + 4) - \gamma(\Lambda D_{\min}, \mu + l + 4)]}{[\gamma(\Lambda D_{\max}, \mu + 4) - \gamma(\Lambda D_{\min}, \mu + 4)]}, \quad (16)$$

where  $c_i$  are coefficients representing the drop terminal velocity relation of Brandes et al. (2002). Figure 2 compares retrieved microphysical process parameters using the CG DSD model with that from the MP DSD model (another example is presented in Brandes et al. 2006). Calculations with the disdrometer observations are shown for reference. If the disdrometer results can be considered as "truth," the MP model overestimates evaporation and accretion for stratiform rain by up to a factor of 10 and underestimates them for strong convection. This might be the reason that the parameterization coefficients in (2)–(3) are usually reduced by

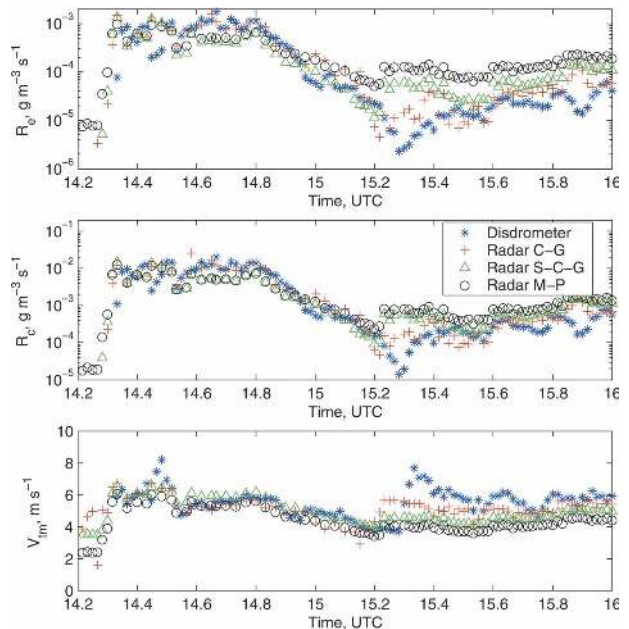


FIG. 2. As in Fig. 1 except for estimated evaporation rate ( $R_e$ ) for a unit vapor saturation deficit, accretion rate ( $R_c$ ) for a unit cloud water content, and mass-weighted terminal velocity ( $V_{tm}$ ).

one-half (or more) in an attempt to improve weather model forecasts (Miller and Pearce 1974; Sun and Crook 1997). The MP model also underestimates the mass-weighted terminal velocity for stratiform rain because the droplet size is underestimated. The MP model yields a smaller dynamic range for all microphysical process parameters, which could be a reason (in addition to grid resolution) that cloud models have difficulty resolving finescale storm features (Seifert and Beheng 2001). It is apparent that the CG DSD model gives more accurate estimation of rain microphysical processes than the MP model. It is because of the use of reflectivity and differential reflectivity (i.e., two parameters) in the retrieval process that the CG rain model more closely represents the disdrometer-derived (natural) raindrop spectra than the single parameter MP model. Therefore, the CG parameterization scheme [(14)–(16)] can be used to improve two-moment models that forecast two microphysical parameters (e.g.,  $W$  and  $D_0$ ). For convenience, the CG parameterization can be expressed in terms of  $W$  and  $D_0$  as

$$R_e = W(-0.1494D_0^3 + 1.109D_0^2 - 2.767D_0 + 2.597) \times 10^{-3} \quad (17)$$

$$R_c = W(0.0161D_0^3 - 0.0139D_0^2 - 1.097D_0 + 6.982) \times 10^{-3} \quad (18)$$

$$V_{tm} = 0.100D_0^3 - 1.133D_0^2 + 5.145D_0 - 0.104. \quad (19)$$

Equations (17)–(19) are alternative forms of (14)–(16), obtained by fitting  $R_e/W$ ,  $R_c/W$ , and  $V_{tm}$  to polynomial functions of  $D_0$ . The fitting results are shown in Fig. 3. The discrete points are calculations from integrations of disdrometer measurements (Zhang et al. 2001; Brandes et al. 2003). There is very little deviation from the fitted curves, suggesting that the two-parameter model accurately represents rain microphysics. Mean relative errors for  $R_e$ ,  $R_c$ , and  $V_{tm}$  estimates with (17)–(19) are less than 6%. (The same approach was applied to polarization radar retrievals and similar results were obtained.) The ratios  $R_e/W$  and  $R_c/W$  decrease as  $D_0$  increases except for  $R_e/W$  at large  $D_0$ . This is because the total surface area and cross section associated with evaporation and accretion are smaller for DSDs dominated by large raindrops than for small drops at the same  $W$ . The flattening of  $R_e/W$  at large  $D_0$  is due to the fact that large  $D_0$ s usually occur in storm centers where DSDs typically have a broad distribution with large numbers of small drops. It is obvious that microphysical process parameters computed from the CG DSD depend on both rainwater content and droplet size, which makes physical sense.

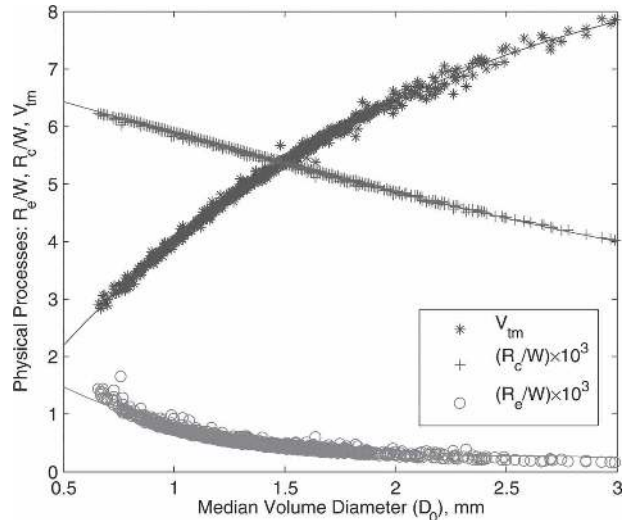


FIG. 3. Dependence of rain microphysical process parameters ( $R_e$ ,  $R_c$ , and  $V_{tm}$ ) on median volume diameter ( $D_0$ ) for CG DSDs. The discrete points are estimates from disdrometer measurements;  $R_e$  and  $R_c$  are in  $\text{g m}^{-3} \text{s}^{-1}$ ,  $W$  in  $\text{g m}^{-3}$ , and  $V_{tm}$  in  $\text{m s}^{-1}$ .

### 3. Simplified constrained-gamma model parameterization

Bulk model parameterization in most numerical simulations using the MP DSD model is typically based on only one parameter, liquid water content, or water mixing ratio. To apply the CG model parameterization, (14)–(16) or (17)–(19), in a numerical model that does not forecast  $D_0$ , we need to reduce the two-parameter model to a single parameter. As we have seen, the CG DSD model and retrievals are represented by two radar measurements, that is, reflectivity and differential reflectivity. It is noted that for rain these measurements are statistically related. The dataset in Fig. 4 was created from calculations of electromagnetic wave scattering for disdrometer measurements collected in east-central Florida during the summer of 1998 field program (PRECIP98) when NCAR's S-band dual-polarization Doppler radar (S-Pol) was deployed (Brandes et al. 2002). A mean relation is derived from the data as follows:

$$Z_{DR} = 10^{(-2.362 \times 10^{-4} Z_H^2 + 0.04581 Z_H - 1.4333)}, \quad (20)$$

where  $Z_H$  is in dBZ and  $Z_{DR}$  is in dB. The  $Z_{DR}$ – $Z_H$  scatterplot, for Florida convective storms, provides information about rain type and microphysics. As indicated in the figure, the data points for moderate and small reflectivity above the mean curve are usually associated with stratiform rain formed from convective

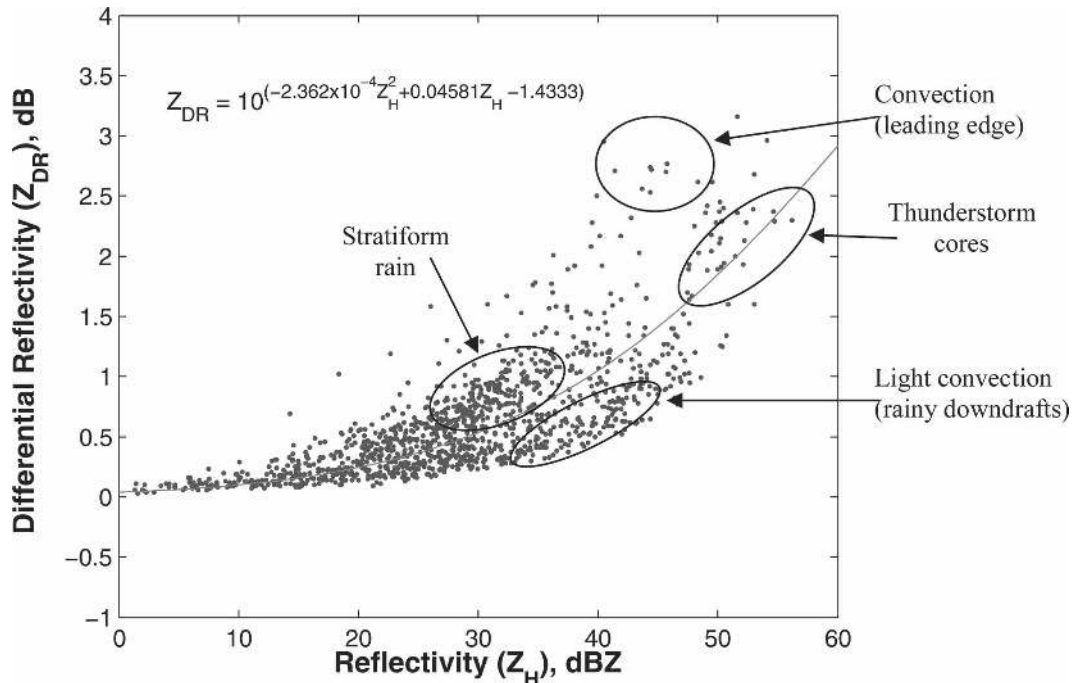


FIG. 4. The statistical relation between radar reflectivity and differential reflectivity for rain. The dataset is obtained from the disdrometer observations collected in east-central Florida during the PRECIP98 project.

debris or with the leading edge of convection where drops are typically large (large  $Z_{DR}$ ). The points with large reflectivity and distributed along the mean curve are characteristic of convective storm cores. Those close to the lower boundary of the data domain are representative of rainy convective downdraft with lots of small drops. Stratiform rain in Florida tends to have small number concentrations and relatively large  $D_0$  compared with light convective rain with the same rainfall rate. These properties are similar to those found by Bringi et al. (2003) and Steiner et al. (2004). Normally, both  $Z_H$  and  $Z_{DR}$  are needed to accurately characterize rain microphysics and physical process. Note, however, with (20) much of the information in the  $Z_{DR}$  measurement is lost; and, consequently, it should be used only in one-moment models.

Substitution of (20) into (9) enables rainwater content estimation from radar reflectivity alone and constitutes a simplified CG (SCG) DSD model. Retrievals of rain microphysical parameters based on the SCG DSD model are shown in Figs. 1 and 2 and are improved over those from the MP DSD model. Rainwater estimates from radar reflectivity using the SCG model and the MP model (5) are compared in Fig. 5. Calculations with disdrometer data are also shown for reference. It is seen that the two estimated water contents agree for the medial radar reflectivity values at which most rain falls, but the SCG DSD model allows

a larger dynamic range of water content and gives a smaller water content for weak radar reflectivity (stratiform rain) than the MP model. The SCG model results agree with disdrometer observations better than the MP model. This is consistent with the results shown in Figs. 1 and 2, which is a subset of data shown in Fig. 5.

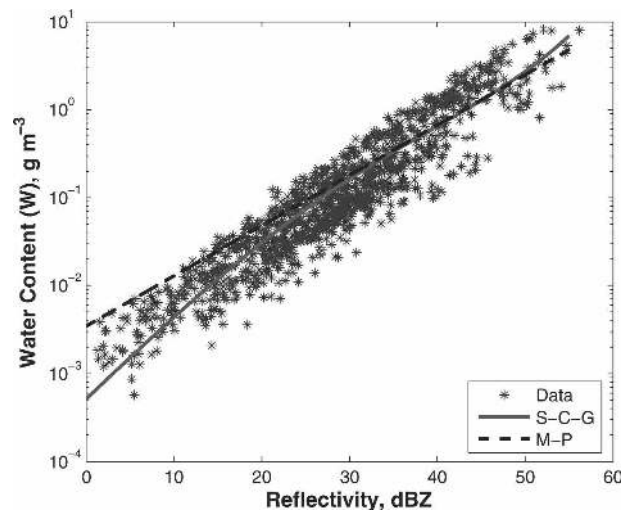


FIG. 5. Comparison of rainwater content estimates using the SCG and MP DSD models.

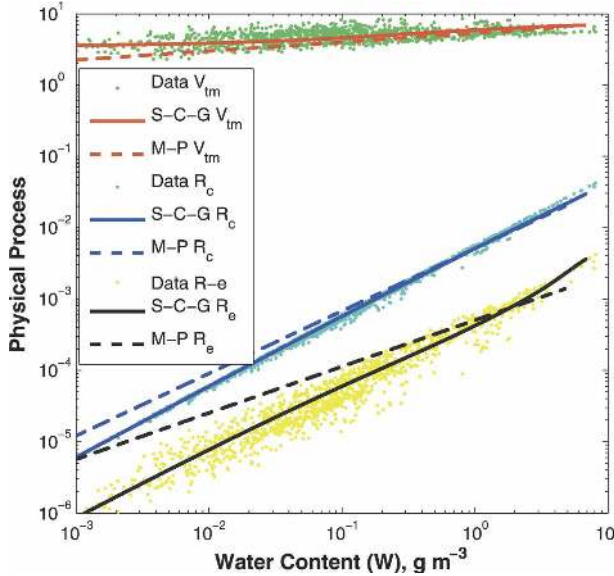


FIG. 6. Comparison of rain physical process parameters between SCG DSD and MP DSD model;  $R_e$  and  $R_c$  are in  $\text{g m}^{-3} \text{s}^{-1}$ , and  $V_{tm}$  is in  $\text{m s}^{-1}$ .

Microphysics process parameters for evaporation, accretion, and mass-weighted terminal velocity are calculated for the SCG DSD model parameterization. The procedure is to (i) estimate  $Z_{DR}$  from  $Z_H$  using (20); (ii) calculate  $W$ ,  $D_0$ ,  $\mu$ , and  $\Lambda$  using (9), (12), (13), and (7), respectively; and (iii) substitute  $W$ ,  $\mu$ , and  $\Lambda$  into (14)–(16) to calculate  $R_e$ ,  $R_c$ , and  $V_{tm}$ . The microphysics process parameters are plotted as a function of rainwater content in Fig. 6. Results for MP DSD model parameterization and that from the direct calculation with the disdrometer data are shown for comparison. It is noted that the SCG DSD model yields smaller evaporation and accretion rates than the MP DSD model for light (stratiform) rain, which agrees with the disdrometer results better. However, the scatter in Fig. 6 is so much larger than that in Fig. 3, indicating that a single parameter cannot accurately characterize rain microphysical processes. Derivatives of the physical process

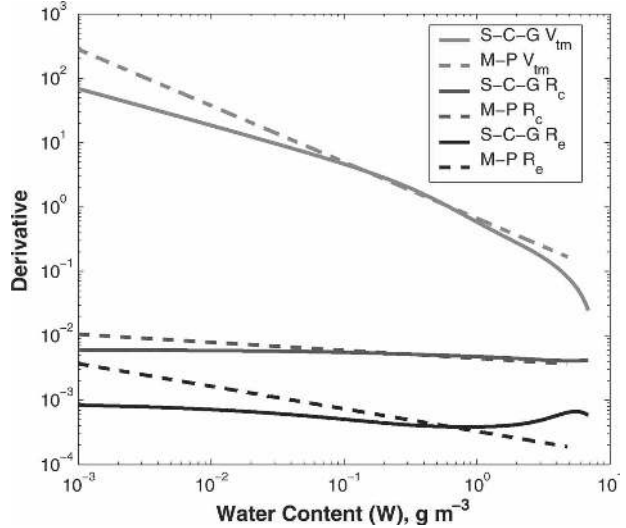


FIG. 7. Derivatives of physical process parameters: evaporation rate ( $dR_e/dW$ ), accretion rate ( $dR_c/dW$ ), and mass-weighted terminal velocity ( $dV_{tm}/dW$ ) for the SCG and MP DSD models.

parameters with respect to the rainwater content are also calculated and shown in Fig. 7 with a logarithmic scale. It is interesting to note that the derivative of evaporation rate approaches a constant for the SCG model rather than a monotonic increase for the MP model when the rainwater content approaches zero. The large derivative resulting from the nonlinearity of the evaporation rate and the terminal velocity for the MP model causes a significant convergence problem in data assimilation, requiring special treatment and approximations to be made in the variational analysis of radar data (Sun and Crook 1997). For example, a constant derivative was forced for rainwater mixing ratios below a specified value. Therefore, the reduced nonlinearity at low water contents in the SCG model parameterization is another advantage over the MP parameterization for data assimilation applications.

For convenience, the microphysical process parameters (14)–(16) constrained by (20) were also fitted to exponent polynomial functions, giving

$$R_e = 10^{[0.00679(\log W)^4 + 0.0557(\log W)^3 + 0.119(\log W)^2 + 0.937 \log W - 3.369]} \quad (21)$$

$$R_c = 10^{[-0.0000603(\log W)^4 - 0.00255(\log W)^3 - 0.0212(\log W)^2 + 0.933 \log W - 2.294]} \quad (22)$$

$$V_{tm} = -4.509 \times 10^{-4}(\log W)^4 + 0.0148(\log W)^3 + 0.263(\log W)^2 + 1.410 \log W + 5.799. \quad (23)$$

Performances of these formulas [(20)–(23)] are quantified by calculating relative bias and errors of their estimates as shown in Table 1. The results with the MP

model [(2)–(5)] are also shown for comparison. The water content ( $W$ ) is estimated from radar reflectivity, and  $R_e$ ,  $R_c$ , and  $V_{tm}$  are estimated from  $W$ . The relative

TABLE 1. Bias and error of rain microphysics estimates with the SCG and MP model. Estimations of microphysical processes:  $R_e$ ,  $R_c$ , and  $V_{tm}$  with the SCG model are generally improved, especially in the logarithm domain (numbers superscripted with asterisks).

Bias and error (%)	Bias: $\frac{\langle X^{(E)} - X^{(M)} \rangle}{\langle X^{(M)} \rangle}$		Error: $\frac{\langle  X^{(E)} - X^{(M)}  \rangle}{\langle X^{(M)} \rangle}$	
Method	SCG	MP	SCG	MP
$W/\log(W)^*$	-13.5/4.2*	-13.1/16.3*	49.5/23.9*	49.4/27.0*
$R_e/\log(R_e)^*$	0.9/1.1*	14.4/7.8*	18.6/3.2*	40.1/8.2*
$R_c/\log(R_c)^*$	-5.4/0.3*	-4.4/2.9*	8.9/0.9*	13.7/3.3*
$V_{tm}/\log(V_{tm})^*$	-4.7/-2.3*	-18/-12.8*	16.7/10.7*	21.7/15.1*

bias and error are calculated in both linear and logarithm domains because the error analysis in linear domain is highly weighted by heavy rain and that in logarithm domain accounts for more contribution from light rain data points. The relative bias and error for water content estimates with the SCG model in the linear domain are comparable to those with the MP model at about 13% bias and 50% error. However, estimations of microphysical processes:  $R_e$ ,  $R_c$ , and  $V_{tm}$  with the SCG model are generally improved, especially in the logarithm domain (numbers superscripted with asterisks). For example, the error of the SCG  $R_e$  estimates is 18.6% in linear domain and 3.2%\* in logarithm domain while that of the MP estimates is 40.1% and 8.2%\*, respectively. The relative bias is also reduced substantially. It is noted that this error analysis is preliminary and further verification is required in the future. The parameterization scheme of (21)–(23) can be applied to any numerical weather model with microphysics characterized by a single parameter; that is, by bulk water content or rainwater mixing ratio.

Figure 8 shows the spatial distributions of the rain microphysical process parameters estimated from NCAR's S-pol radar measurements using the CG, SCG, and MP models. The polarization radar is located at (-9 km, -25 km) from the origin. The radar measurements of reflectivity and differential reflectivity were collected at 0.5 degree of elevation. In general, the CG model gives a larger dynamic range, and more detailed features, and larger spatial variations for  $R_e$  and  $R_c$  than the MP model. Results for the SCG model are between that for the CG and MP models. The MP model overestimates evaporation by about three times for the stratiform rain in the upper-right corner of the images. The SCG model gives stratiform rain evaporation close to that of the CG model.

#### 4. Impact of the SCG parameterization on forecasting of storm evolution

The parameterization scheme (21)–(23) with the autoconversion term kept the same was implemented

in the warm cloud model developed by Sun and Crook (1997). A case of Florida multicell storms observed during PRECIP98 was used to test whether the new parameterization scheme improves the forecasting of storms over the MP parameterization scheme (2)–(4). This cloud model is chosen for our study because it has a 4DVAR radar data assimilation system for model initialization. The system is referred to as VDRAS. It has the ability to retrieve the dynamical and microphysical variables needed for initialization and has reasonable skill for very short-term forecasting of storm evolution (Sun and Crook 1998; Wu et al. 2000; Warner et al. 2000; Sun 2005).

The numerical model in VDRAS is anelastic with Kessler-type warm rain microphysical parameterization. There are six prognostic equations: one for each of the three velocity components ( $u$ ,  $v$ , and  $w$ ), the liquid water potential temperature ( $\theta_l$ ), the total water mixing ratio ( $q_t$ ), and the rainwater mixing ratio ( $q_r = W/\rho$ , where  $\rho$  is the air density). The pressure ( $p$ ) is diagnosed through a Poisson equation. The temperature ( $T$ ) and the cloud water mixing ratio ( $q_c$ ) are diagnosed from the prognostic variables ( $\theta_b$ ,  $q_t$ , and  $q_r$ ) by assuming that all vapor in excess of the saturation value is converted to cloud water. The lateral boundary conditions of the numerical model are open, such that the inflow is prescribed and the outflow is extrapolated using the values at the closest two inner grid points. The top and bottom boundary conditions for vertical velocity are set to zero, and all other variables are defined such that their normal derivatives vanish. A simple constant diffusion scheme is used to parameterize turbulence and to maintain numerical stability.

The 4DVAR scheme in VDRAS assimilates a series of consecutive volumes of radar radial velocity and rainwater content (converted from radar reflectivity) within a specified assimilation window. By iteratively adjusting the initial state of the model, a cost function measuring the difference between the model forecast and observations is reduced such that the forecast



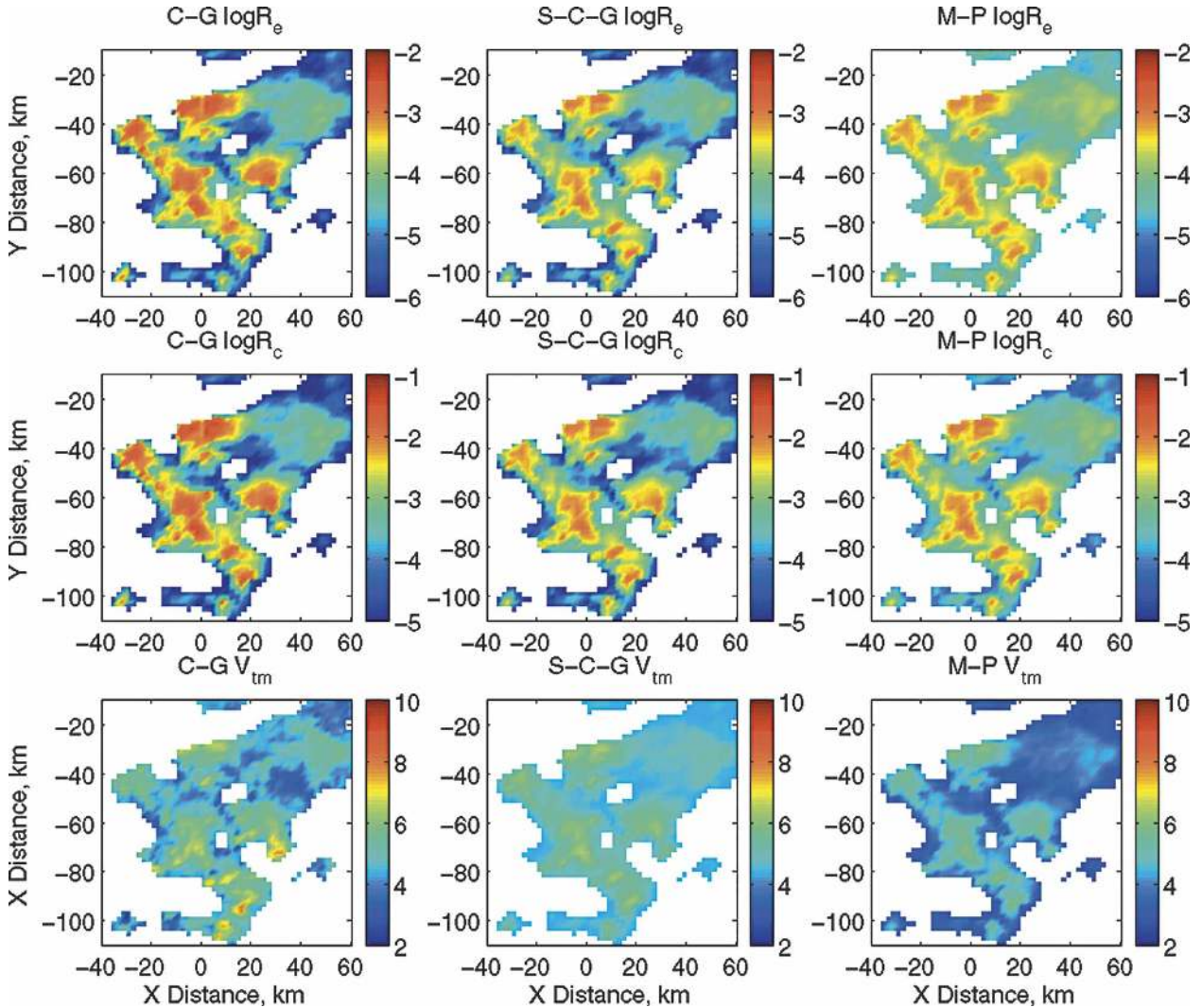


FIG. 8. Comparison of microphysical parameterizations estimated from radar observations using the CG, SCG, and MP models. The data were collected on 2 Sep 1998 with NCAR’s S-pol radar.

matches the observations as closely as possible. The cost function is defined as

$$J = (x_0 - x_b)^T B^{-1} (x_0 - x_b) + \sum_{\sigma,t} [\eta_v (v_r - v_r^o)^2 + \eta_w (W - W^o)^2] + J_p, \quad (24)$$

where  $x_0$  represents the model state at the beginning of the assimilation window and  $x_b$  represents the large-scale background (e.g., an analysis using all observations other than radar observations). The symbol  $B$  denotes the background covariance matrix and is assumed diagonal and constant in this study. The variable  $v_r$  is the radial velocity computed from the model velocity components;  $v_r^o$  is the observed radial velocity;  $W$  is the modeled rainwater content; and  $W^o$  is the rain-

water content estimated from radar reflectivity. The terms  $\eta_v$  and  $\eta_w$  are weighting coefficients for radial velocity and water content and are assumed to be constant. To have comparable contributions from the radial velocity and water content terms,  $\eta_v = 1$  and  $\eta_w = 100$  in this study. The symbol  $J_p$  denotes the spatial and temporal smoothness penalty term. The function of the penalty term is to ensure a smooth fit to the observations. Its exact form can be found in Sun and Crook (2001). Minimization of (24) requires knowledge of the gradient of the cost function, which is provided by the adjoint of the forecast model. The SCG model parameterization for rain microphysical processes (21)–(23) is used in the forecast model and their adjoint is derived to give the gradient for the variational analysis.

The simulation domain is a region of  $140 \times 140 \times 15$  km<sup>3</sup> with  $70 \times 70 \times 30$  grid points. The cloud model is initialized by assimilating radar data from the Melbourne, Florida, Weather Surveillance Radar-1988 Doppler (WSR-88D; KMLB). (For this storm, volumetric measurements with the polarization radar were not available.) Thunderstorms examined here formed in central Florida on 2 September as part of an outer rainband associated with Hurricane Earl. Three volumetric datasets at 2310, 2315, and 2320 UTC, when the storms were most intense, are used for model initialization with the 4DVAR technique. Figure 9 shows the model domain and the locations of the KMLB and S-pol radars, and a sounding site at the Kennedy Space Center. The observed radial velocity (color) and reflectivity (contour) from KMLB are also shown in Fig. 9. The radar data were edited to eliminate contamination caused by insects and ground clutter. Radar reflectivities ( $Z_H > 5$  dBZ) were converted to rainwater contents using (9) and (20) for the SCG model and (5) for the MP model. The first guess (and background) of the 4DVAR data assimilation is from a sounding released at 1900 UTC (Fig. 10).

The initial conditions were found iteratively until a step change of the cost function fell below a threshold value. It took 117/105 iterations for the SCG/MP mod-

els. The initial condition from the 4DVAR was then used to make forecasts with SCG and MP microphysical parameterizations. The model rainwater contents are converted to radar reflectivities by solving inversion problems of (9) and (20) for SCG model and (5) for the MP model (using the two curves in Fig. 5). Figure 11 shows the reflectivity results at the first model level (0.25 km above ground) for the initialization time (2320 UTC) and for 15-, 30-, 45-, and 60-min forecasts (2335, 2350, 0005, and 0020 UTC, respectively). The retrieved wind field at the initialization time and the forecast wind are overlaid on the reflectivity field. The left (right) column presents results for the SCG model (MP model) parameterization. The radar observations are shown in the middle column for comparison.

Before examining the impact of microphysical parameterization on model forecasts some issues associated with the 4DVAR analysis need to be discussed. Insertion of radar observations into the background field shocks the system creating poorly represented convergence and divergence regions that take some time to dampen out. Regions of weak precipitation seen primarily in the initialization for the SCG simulation but not in the radar measurements are a manifestation of this problem and because of the small contribution to the cost function. Note that the spurious precipitation rapidly dissipates. As discussed below, the problem is less evident with the MP parameterization. The apparent better initialization with the MP model could be due to a wrong reason of overestimation for evaporation. If we look at the region for the reflectivity  $>20$  dBZ, the SCG model results agree with the observation better than that with the MP model. It is expected that the effect of the false weak precipitation on the forecasts is small because the rainwater content in these regions is very low ( $<0.03$  g m<sup>-3</sup>). Neither of the model simulations forecast the storms that develop in the southern half of the data domain. The sources causing the storms were not fully included in model initialization. The new convection may have modified the inflow air to the storms in the northern portion of the data domain. It is difficult to quantify the impact these storms had on the observed convection and their absence had on the model simulation.

Our results suggest that the SCG model parameterization has several advantages over the MP DSD model. Stratiform precipitation in the upper-right corner is better represented in the model initialization and is better preserved in the forecasts. This is because the SCG parameterization leads to smaller evaporation and accretion rates, as discussed in the previous section. Also, the linearity at low evaporation (a constant derivative) with the SCG model allows better conver-

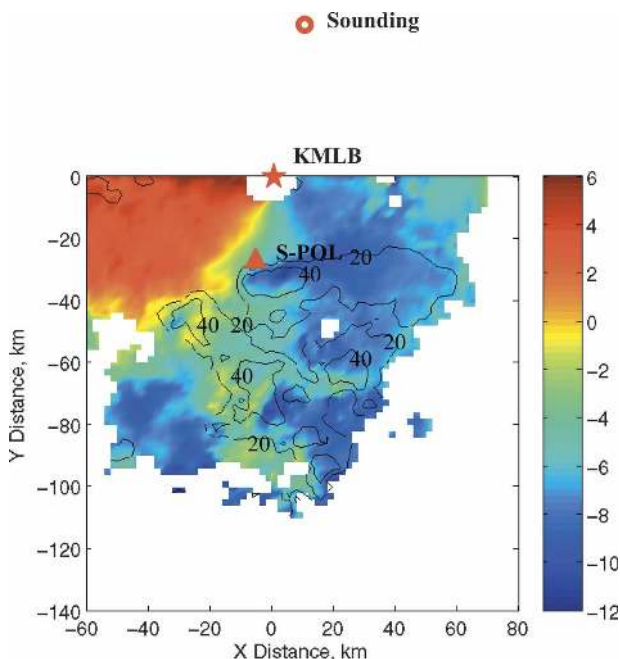


FIG. 9. Configuration of observation systems [sounding, WSR-88D (KMLB), S-Pol] and the simulation domain. It shows radial velocity in  $\text{m s}^{-1}$  (color) and reflectivity (contour at 20 and 40 dBZ) measured by KMLB at 2320 UTC.

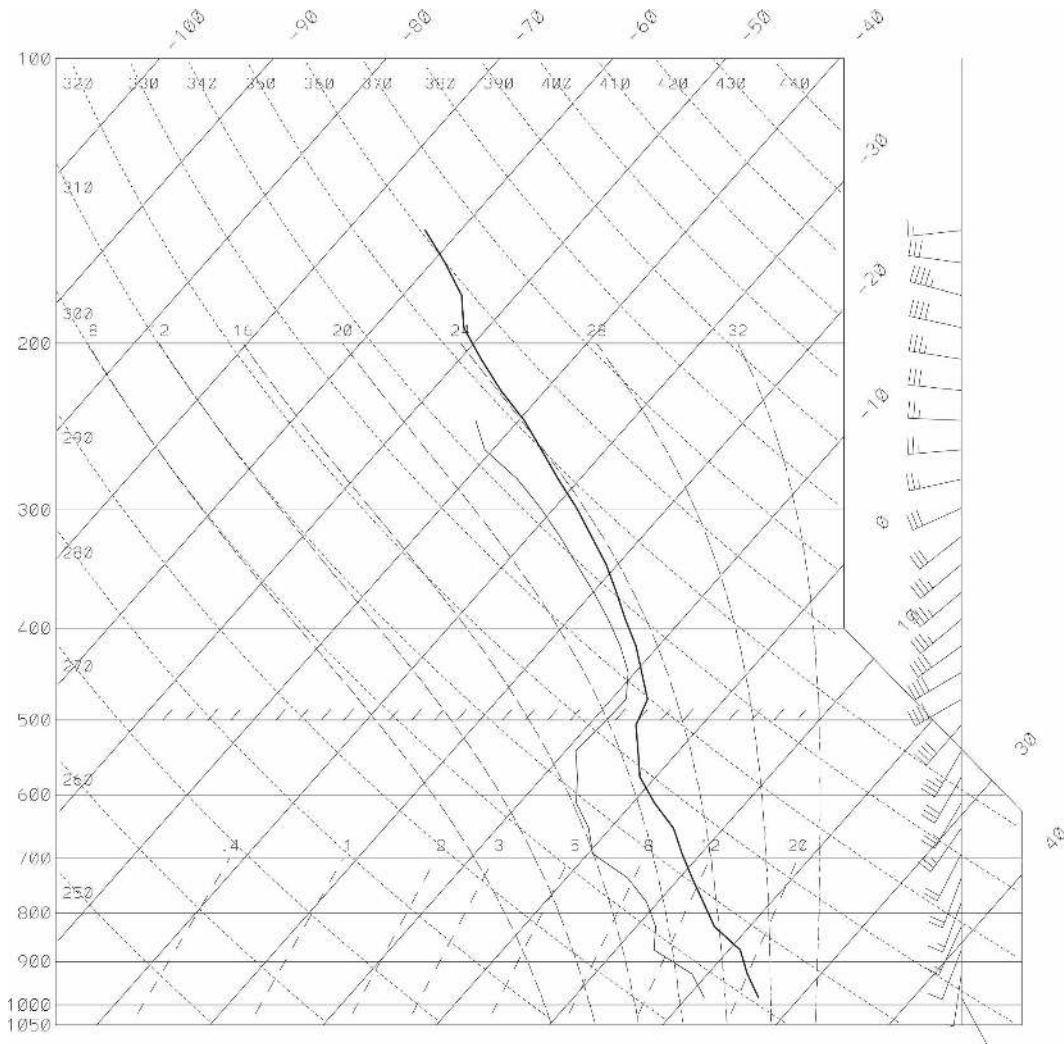


FIG. 10. Skew- $T$  diagram for initial temperature, pressure, and wind profiles. The sounding data was collected at Kennedy Space Center at 1900 UTC, 4 h and 20 min before the model starting time.

gence in the minimization and a more accurate fit with observations. The SCG model forecasts of convective cores (intensity) agree with radar observations better than the MP model. The MP model tends to overpredict rain intensity in the storm core while underforecasting the total storm coverage due to a rapid decay of the stratiform rain, as shown in Fig. 11. To better illustrate the differences of the forecast storm intensity between the two parameterization schemes, the maximal reflectivity factors and forecast rainwater contents for cells 1 to 5 are listed in Table 2. It is clear that the forecast reflectivity using the SCG parameterization is significantly closer to the observed reflectivity for all cells except for cell 4. The difference in the predicted reflectivity values is due to overpredicted water contents by the MP model and different  $W$ - $Z$  relations used in the SCG and MP model. Perhaps this is a result

of higher evaporation in convective storm cores with the SCG model. In Fig. 12, we compare rainwater contents from radar estimates and model forecasts at the first level for the 30-min forecast. The forecast results are shown for a threshold of  $W > 0.001 \text{ g m}^{-3}$ . The upper-left panel is the water content estimated from polarization radar (S-Pol) measurements of  $Z$  and  $Z_{DR}$  using Eq. (9). The upper-right panel is reflectivity-based rainwater estimates from KMLB radar with Eq. (5). The SCG model forecasted water contents are consistent with the S-Pol radar estimates from reflectivity and differential reflectivity. The MP model results do not agree with radar estimates from either dual-polarization measurements or reflectivity only. Clearly, the SCG forecasts agree with radar estimates better the MP model in terms of both coverage and intensity.

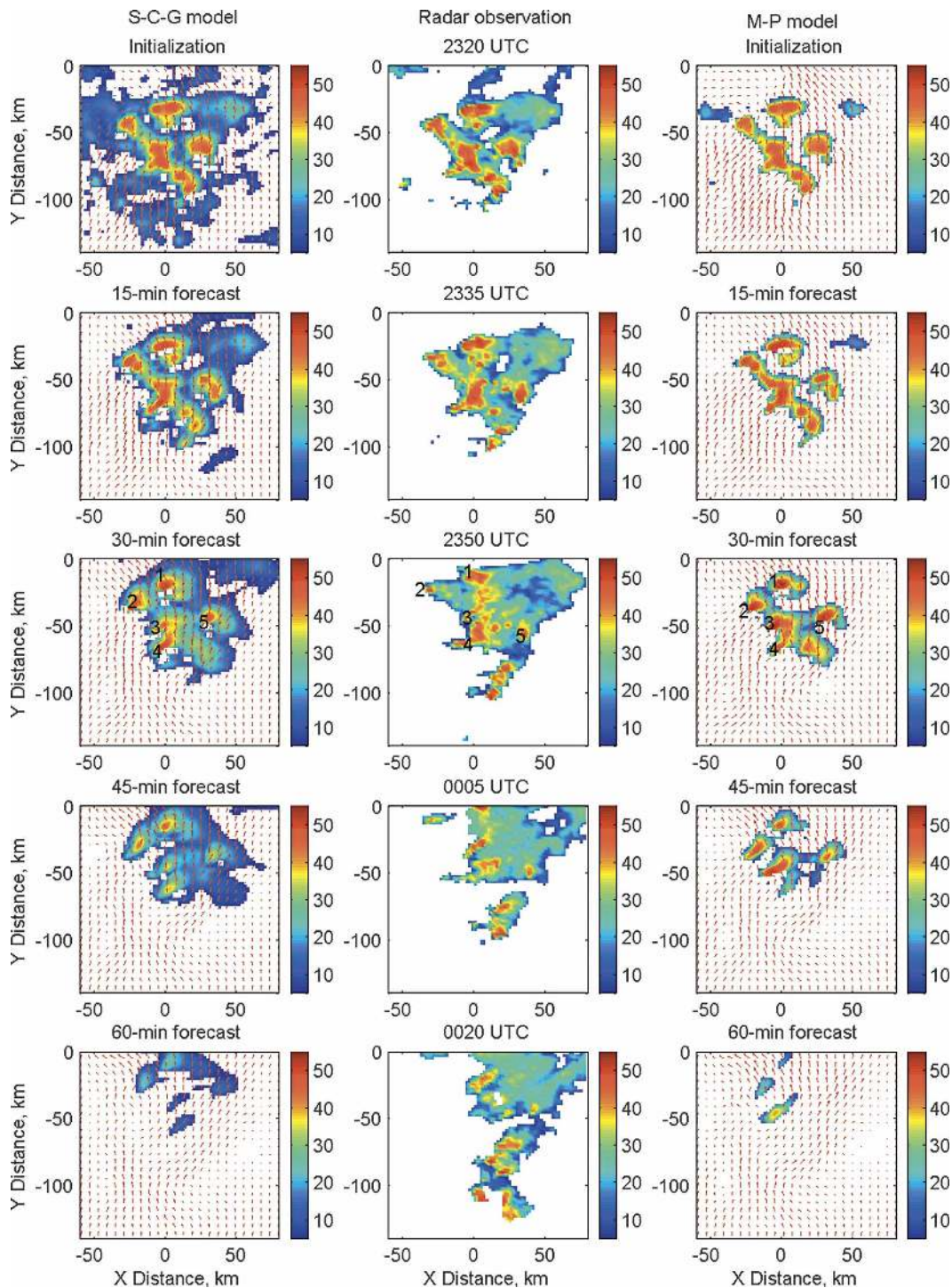


FIG. 11. Numerical weather forecasts based on (left) SCG and (right) MP model parameterizations. Radar observations are shown in the middle column for comparison. Rows show the model and observed reflectivity field at initialization (2320 UTC) and for 15-, 30-, 45-, and 60-min forecasts (2335, 2335, 2350, 0005, and 0020 UTC).

To show the vertical structure of the storm, results at  $y = -30$  km at initialization and for 30-min forecasts are plotted in Fig. 13. A radar bright band was not evident in this warm rain system. Both the SCG and MP

model initializations have background residual precipitation in the left-hand portions of the images, but the SCG model initialization and forecasts agree with observations better than the MP model for rain aloft and

TABLE 2. Comparison of 30-min forecasts between the SCG and MP model parameterizations

Observation or forecast	Radar observation	SCG model		MP model	
Parameters	$Z$ , dBZ	$Z$ , dBZ	$W$ , $\text{g m}^{-3}$	$Z$ , dBZ	$W$ , $\text{g m}^{-3}$
Cell 1	47.7	50.9	3.12	55.8	5.35
Cell 2	46.1	46.7	1.67	53.3	3.81
Cell 3	44.4	43.9	1.11	54.1	4.23
Cell 4	47.4	49.8	2.65	48.3	1.98
Cell 5	46.4	47.6	1.90	52.1	3.28

near the ground. The high evaporation rate in the MP model parameterization causes fast decay of rain with low water content and prevents some stratiform rain from reaching the ground (e.g., in Fig. 11 for all forecasts and in Fig. 13 for the 30-min forecast). The SCG model results are more accurate and reasonable in characterizing the spatial precipitation distribution and storm evolution than the MP model. A number of columnar precipitation rainouts can be seen in Figs. 11 and 13 (e.g., see large gradients at the edge of some convective cores). Rainouts, believed to be caused by inconsistencies in the numerical model system associated with gradients, occur less frequently with the SCG

model. To quantify the forecast results, Fig. 14 shows the frequency distribution of reflectivity values ( $Z > 15$  dBZ) of 2350 UTC at height of 0.25, 2.75, and 5.25 km (Yuter and Houze 1995). Histograms are shown for both radar observations and model forecasts. In general, the forecast results with the SCG model agree with radar observations better than the MP model results.

## 5. Summary and discussion

This paper presents a parameterization scheme for rain microphysical processes based on a constrained-gamma DSD model developed from disdrometer and

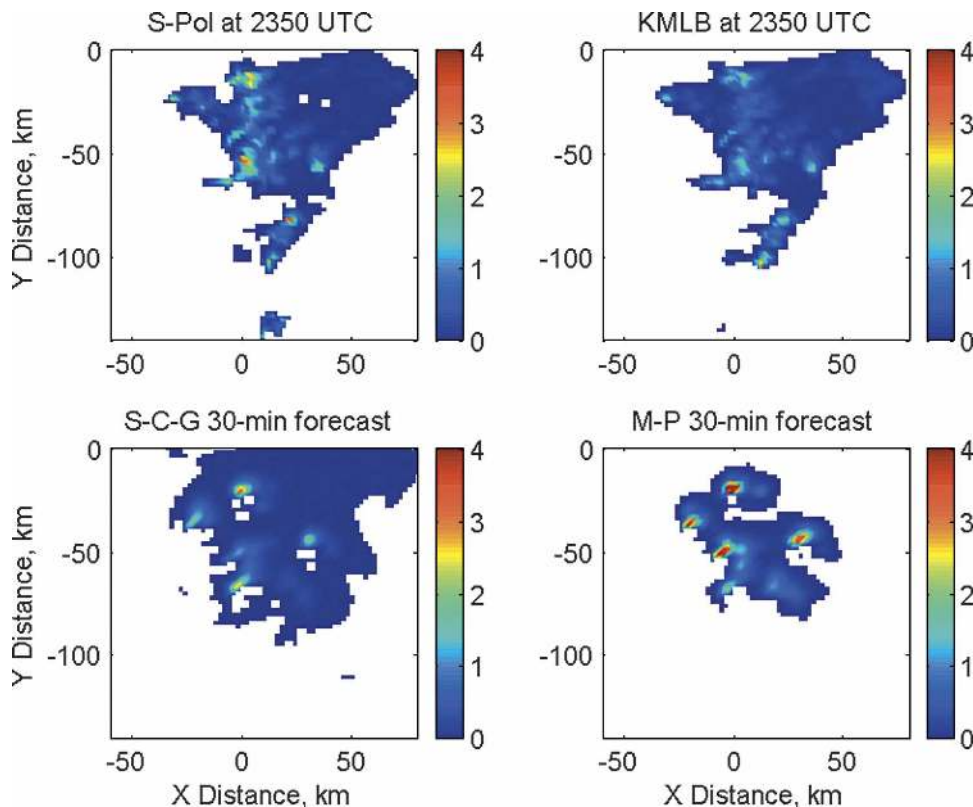


FIG. 12. Comparison of rainwater content ( $\text{g m}^{-3}$ ) from radar estimates and model forecasts for the first level at 2350 UTC.

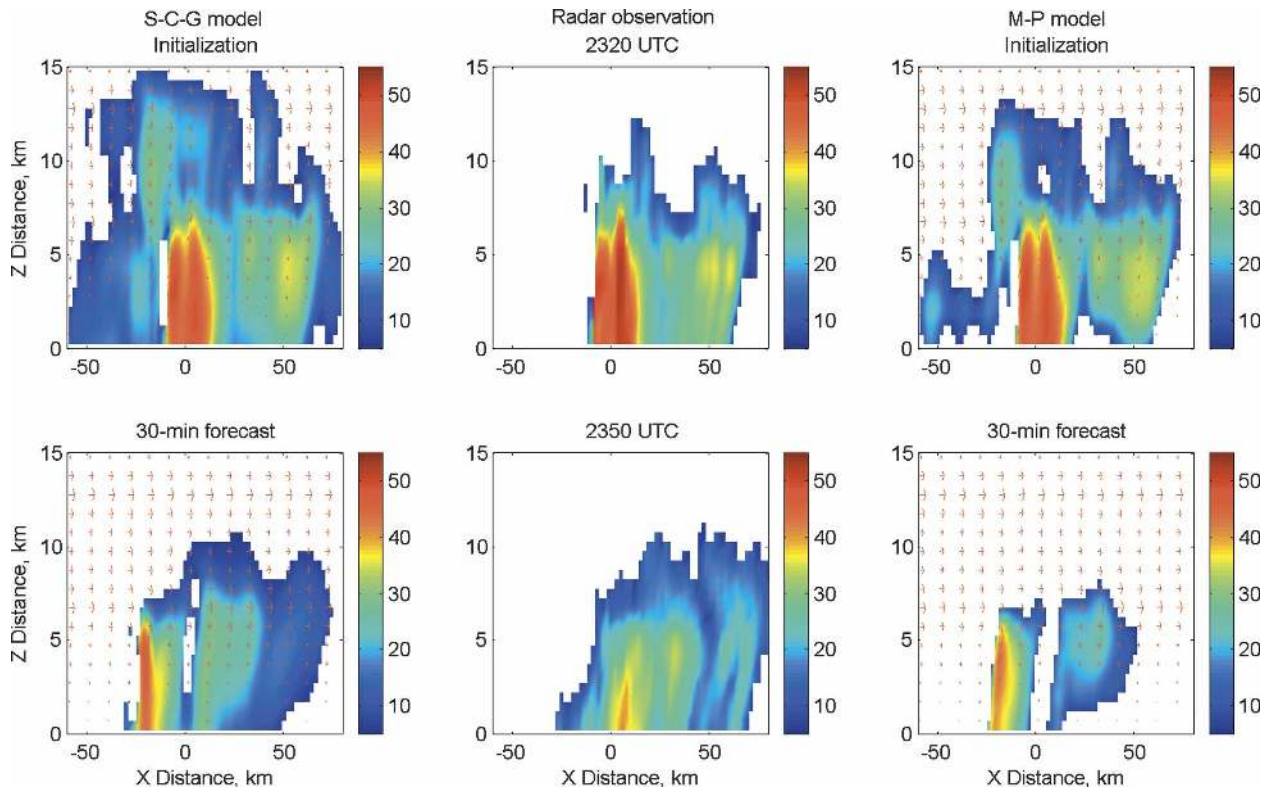


FIG. 13. As in Fig. 11 except for vertical profiles at  $Y$  distance of  $-30$  km at initialization, and for 30-min forecasts.

polarization radar observations. The CG DSD model yields smaller evaporation and accretion rates as well as their derivatives than the MP model for stratiform rain, and higher  $R_e$  and  $R_c$  in the core regions of convective storms. The CG model parameterization was further simplified to a single-parameter scheme (SCG) in which the microphysical process parameters are expressed by polynomial functions of rainwater content. The exponent polynomial form has better performance (continuity and linearity) at lower water contents than the power-law form of the MP model. The SCG model parameterization produces better variational analysis for model initialization and better short-term forecasts for warm rain processes by (i) preserving the stratiform component of the precipitation and (ii) predicting the intensity of convective cores more accurately than MP model parameterization. This is because the SCG model yields less (more) evaporation and accretion than the MP model at low (high) rainwater content.

Parameterization coefficients have often been empirically adjusted to produce better forecasts. Such adjustments may be applicable because evaporation, accretion, and precipitation also depend on temperature, humidity, and storm dynamical processes that are not

included in microphysical parameterization and because of smoothing effects in model simulation. Reducing the evaporation and accretion terms may improve forecast results, but the problems associated with the nonlinear power-law functions remain. It is important to have the correct functional forms for the microphysical process parameters before adjusting their coefficients. Accurate microphysical parameterization based on advanced measurement techniques such as polarization radar observations and disdrometer measurements is highly desirable and feasible. Because radar provides large coverage weather observations and a 2D video disdrometer measures ground truth, a combination of polarization radar and disdrometer measurements makes observation-based model parameterization reliable and useful.

The CG and SCG model parameterizations derived in this study can be applied to two-moment and one-moment numerical weather models, respectively. We applied the SCG model parameterization in VDRAS in this study because volumetric polarization radar data were not available and a two-moment data assimilation system has not been developed. The SCG model parameterization is a single-moment parameterization, much like the MP model, without adding an additional

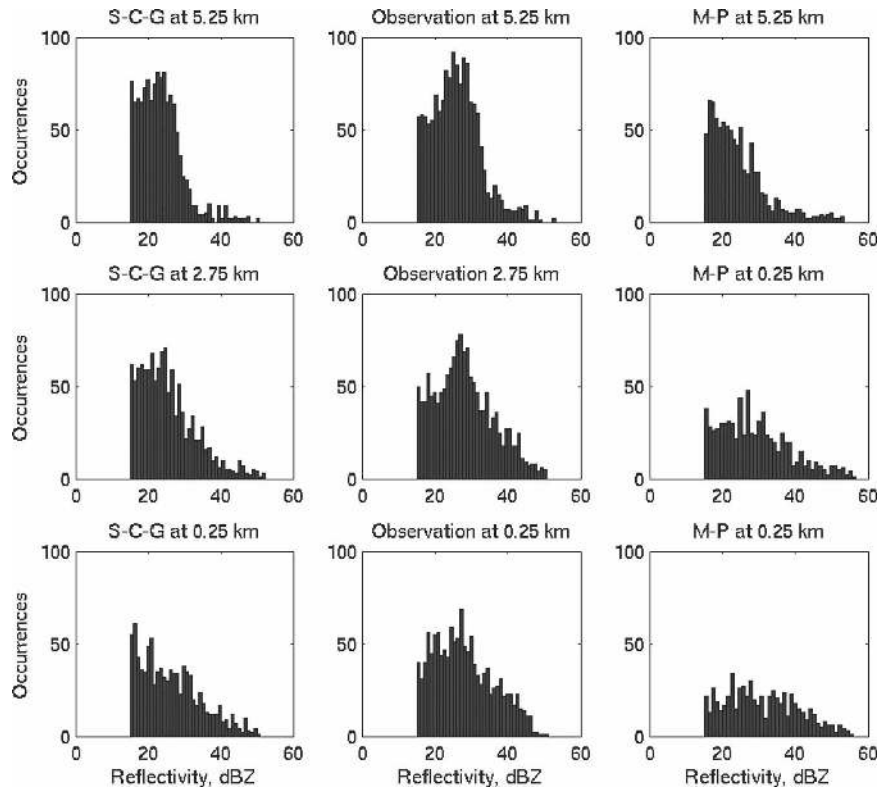


FIG. 14. Histograms of reflectivity values at heights of 0.25, 2.75, and 5.25 km for radar observations and model forecasts. The results are for 2350 UTC, 30-min forecasts.

variable to a numerical model. The application of the SCG model in VDRAS is just the first step in using the CG model in NWP. The results shown in this paper are not necessarily the best, as there are many factors affecting model forecasting. Nevertheless, it has been shown that (i) the single-parameter SCG model yields better model initialization and forecast results than the MP model, and (ii) the two-parameter CG model has potential to further improve NWP. Future work will be on applying the CG parameterization to a two-moment numerical weather model so that both radar reflectivity and differential reflectivity are used to characterize rain microphysics, to initialize the model, and to verify the forecast.

*Acknowledgments.* The research was supported by NCAR Director's Opportunity Fund and by funds from the National Science Foundation that have been designated for U.S. Weather Research Program activities at the National Center for Atmospheric Research (NCAR). We sincerely appreciate helpful discussions with Ms. Ying Zhang, Drs. Frederick H. Carr, Kelvin K. Droegemeier, Jerry Straka, Ming Xue, and Dusan S. Zrnica.

## APPENDIX

### Derivation of Rain Microphysical Process Parameters for the Constrained-Gamma Drop Size Distribution

Rain microphysical process parameters: evaporation rate ( $R_e$ ), accretion rate ( $R_c$ ), and mass-weighted terminal velocity ( $V_{tm}$ ) depend on the rain drop size distribution (DSD). For a given rain DSD, such as constrained-gamma model, the microphysical processes can be represented by the DSD parameters or model forecasting parameters (rainwater content and droplet size). Following Kessler (1969) and Brandes et al. (2006), the parameters  $R_e$ ,  $R_c$ , and  $V_{tm}$  are derived as follows.

#### a. Evaporation rate ( $R_e$ )

As given in Eq. (8.28) of Kessler (1969), the rate of evaporation of a single raindrop is rewritten with a unit conversion as

$$\frac{\delta M_e}{\delta t} = 3.55 \times 10^{-7} E_e m_e D^{8/5} (D \text{ in mm}), \quad (\text{A1})$$

where the evaporation coefficient is  $E_e$ ,  $D$  is the rain-drop diameter, and  $m_e$  is the vapor saturation deficit.

Integrating (A1) over all diameters  $[D_{\min}, D_{\max}]$  for a gamma DSD (6) yields the rainwater evaporation rate as

$$\begin{aligned}
 R_e &= \int_{D_{\min}}^{D_{\max}} \frac{\delta M_e}{\delta t} N(D) dD \\
 &= 3.55 \times 10^{-7} E_e m_e N_0 \int_{D_{\min}}^{D_{\max}} D^{\mu+8/5} \exp(-\Lambda D) dD \\
 &= 3.55 \times 10^{-7} E_e m_e N_0 \Lambda^{-(\mu+13/5)} [\gamma(\Lambda D_{\max}, \mu + 13/5) - \gamma(\Lambda D_{\min}, \mu + 13/5)]. \tag{A2}
 \end{aligned}$$

Replacing  $N_0$  in (A2) with  $W$  using (8), we obtain

$$\begin{aligned}
 R_e &= 3.55 \times 10^{-7} \frac{6W\Lambda^{(\mu+4)}}{\rho_w \times 10^{-3} \pi [\gamma(\Lambda D_{\max}, \mu + 4) - \gamma(\Lambda D_{\min}, \mu + 4)]} \\
 &\quad \times E_e m_e \Lambda^{-(\mu+13/5)} [\gamma(\Lambda D_{\max}, \mu + 13/5) - \gamma(\Lambda D_{\min}, \mu + 13/5)] \\
 &= 6.78 \times 10^{-4} E_e m_e W \Lambda^{7/5} \frac{[\gamma(\Lambda D_{\max}, \mu + 13/5) - \gamma(\Lambda D_{\min}, \mu + 13/5)]}{[\gamma(\Lambda D_{\max}, \mu + 4) - \gamma(\Lambda D_{\min}, \mu + 4)]} \text{ (g m}^{-3} \text{ s}^{-1}) \tag{A3}
 \end{aligned}$$

*b. Accretion rate ( $R_c$ )*

Accretion is the cloud water swept out and accumulated by raindrops. The rate of accretion for a single raindrop is given by Kessler (1969) in the Eq. (8.21) as

$$\frac{\delta M_c}{\delta t} = 10^{-6} \frac{\pi D^2}{4} E_c(D) v(D) m_c(D \text{ in mm}), \tag{A4}$$

where the collection efficient is  $E_c(D)$ ,  $v(D)$  is the falling velocity of the raindrop, and  $m$  is the cloud water content. The collection efficiency  $E(D)$  is usually as-

sumed to be constant. The terminal velocity is that of Brandes et al. (2002)

$$\begin{aligned}
 v &= -0.1021 + 4.932D - 0.9551D^2 + 0.07934D^3 \\
 &\quad - 0.002362D^4 = \sum_{l=0}^4 c_l D^l. \tag{A5}
 \end{aligned}$$

Substituting (A5) into (A4), integrating the gamma DSD (6) over all diameters, and replacing  $N_0$  with  $W$  using (8), we obtain the accretion rate as

$$\begin{aligned}
 R_c &= \int_{D_{\min}}^{D_{\max}} \frac{\delta M_c}{\delta t} N(D) dD \\
 &= 10^{-6} \int_{D_{\min}}^{D_{\max}} \frac{\pi D^2}{4} E_c(D) v(D) m_c N(D) dD \\
 &= \frac{\pi}{4} \times 10^{-6} E m_c N_0 \int_{D_{\min}}^{D_{\max}} D^2 \sum_{l=0}^4 c_l D^{\mu+l} \exp(-\Lambda D) dD \\
 &= \frac{\pi}{4} \times 10^{-6} E_e m_c \frac{6W\Lambda^{(\mu+4)}}{\rho_w \times 10^{-3} \pi [\gamma(\Lambda D_{\max}, \mu + 4) - \gamma(\Lambda D_{\min}, \mu + 4)]} \\
 &\quad \times \sum_{l=0}^4 c_l \Lambda^{-(\mu+l+3)} [\gamma(\Lambda D_{\max}, \mu + l + 3) - \gamma(\Lambda D_{\min}, \mu + l + 3)] \\
 &= \frac{3}{2} \times 10^{-3} E_e m_c W \sum_{l=0}^4 c_l \Lambda^{-l+1} \frac{[\gamma(\Lambda D_{\max}, \mu + l + 3) - \gamma(\Lambda D_{\min}, \mu + l + 3)]}{[\gamma(\Lambda D_{\max}, \mu + 4) - \gamma(\Lambda D_{\min}, \mu + 4)]} \text{ [g m}^{-3} \text{ s}^{-1}]. \tag{A6}
 \end{aligned}$$



### c. Mass-weighted terminal velocity ( $V_{tm}$ )

The mass-weighted terminal velocity for a gamma rain DSD model is calculated from its definition and (A5) as follows:

$$\begin{aligned}
 V_{tm} &= \frac{\int_{D_{\min}}^{D_{\max}} D^3 v(D) N(D) dD}{\int_{D_{\min}}^{D_{\max}} D^3 N(D) dD} \\
 &= \frac{\sum_{l=0}^4 c_l \int_{D_{\min}}^{D_{\max}} D^{l+3} N(D) dD}{\int_{D_{\min}}^{D_{\max}} D^3 N(D) dD} \\
 &= \frac{\sum_{l=0}^4 c_l \int_{D_{\min}}^{D_{\max}} D^{\mu+l+3} \exp(-\Lambda D) dD}{\int_{D_{\min}}^{D_{\max}} D^{\mu+3} \exp(-\Lambda D) dD} \\
 &= \sum_{l=0}^4 c_l \Lambda^{-l} \frac{[\gamma(\Lambda D_{\max}, \mu + l + 4) - \gamma(\Lambda D_{\min}, \mu + l + 4)]}{[\gamma(\Lambda D_{\max}, \mu + 4) - \gamma(\Lambda D_{\min}, \mu + 4)]} [\text{m s}^{-1}]. \tag{A7}
 \end{aligned}$$

Hence, (A3), (A6), and (A7) constitute microphysical parameterization based on a gamma rain DSD model.

### REFERENCES

- Brandes, E. A., G. Zhang, and J. Vivekanandan, 2002: Experiments in rainfall estimation with a polarimetric radar in a subtropical environment. *J. Appl. Meteor.*, **41**, 674–685.
- , —, and —, 2003: An evaluation of a drop distribution-based polarimetric radar rainfall estimator. *J. Appl. Meteor.*, **42**, 652–660.
- , —, and —, 2004a: Drop-size distribution retrieval with polarimetric radar: Model and application. *J. Appl. Meteor.*, **43**, 461–475.
- , —, and —, 2004b: Comparison of polarimetric radar drop size distribution retrieval algorithms. *J. Atmos. Oceanic Technol.*, **21**, 584–598.
- , —, and J. Sun, 2006: On the influence of assumed drop size distribution form on retrieved thunderstorm microphysics. *J. Appl. Meteor. Climatol.*, **45**, 259–268.
- Bringi, V. N., V. Chandrasekhar, J. Hubbert, E. Gorgucci, W. L. Randeu, and M. Schoenhuber, 2003: Raindrop size distribution in different climatic regimes from disdrometer and dual-polarized radar analysis. *J. Atmos. Sci.*, **60**, 354–365.
- Chen, J.-P., and S.-T. Liu, 2004: Physically based two-moment bulkwater parameterization for warm-cloud microphysics. *Quart. J. Roy. Meteor. Soc.*, **130**, 51–78.
- Clark, T. L., 1977: A small-scale dynamic model using a terrain-following coordinate transformation. *J. Comput. Phys.*, **24**, 186–215.
- Droegemeier, K. K., and Coauthors, 2000: Hydrological aspects of weather prediction and flood warnings: Report of the Ninth Prospectus Development Team of the U.S. Weather Research Program. *Bull. Amer. Meteor. Soc.*, **81**, 2665–2680.
- Ferrier, B. S., 1994: A double-moment multiple-phase 4-class bulk ice scheme. Part I: Description. *J. Atmos. Sci.*, **51**, 249–280.
- Hagen, M., and S. E. Yuter, 2003: Relations between radar reflectivity, liquid-water content, and rainfall rate during the MAP SOP. *Quart. J. Roy. Meteor. Soc.*, **129**, 477–493.
- Hong, S.-Y., J. Dudhia, and S.-H. Chen, 2004: A revised approach to ice microphysical processes for the bulk parameterization of clouds and precipitation. *Mon. Wea. Rev.*, **132**, 103–120.
- Kessler, E., 1969: *On the Distribution and Continuity of Water Substance in Atmospheric Circulations*. Meteor. Monogr., No. 32, Amer. Meteor. Soc., 84 pp.
- Klemp, J. B., and R. B. Wilhelmson, 1978: The simulation of three-dimensional convective storm dynamics. *J. Atmos. Sci.*, **35**, 1070–1096.
- Lin, Y.-L., R. D. Farley, and H. D. Orville, 1983: Bulk parameterization of the snow field in a cloud model. *J. Climate Appl. Meteor.*, **22**, 1065–1092.
- Liu, Y. Y., and P. H. Daum, 2004: Parameterization of the auto-conversion process. Part I: Analytical formulation of the Kessler-type parameterizations. *J. Atmos. Sci.*, **61**, 1539–1548.
- Marshall, J. S., and W. McK. Palmer, 1948: The distribution of raindrops with size. *J. Meteor.*, **5**, 165–166.
- Meyers, M. P., R. L. Walko, J. Y. Harrington, and W. R. Cotton, 1997: New RAMS cloud microphysics parameterization. Part II: The two-moment scheme. *Atmos. Res.*, **45**, 3–39.
- Miller, M. J., and R. P. Pearce, 1974: A three-dimensional primitive equation model of cumulonimbus convection. *Quart. J. Roy. Meteor. Soc.*, **100**, 133–154.
- Rutledge, S. A., and P. V. Hobbs, 1983: The mesoscale and microscale structure and organization of clouds and precipitation in midlatitude cyclones. Part VIII: A model for the

- “seeder-feeder” process in warm-frontal rainbands. *J. Atmos. Sci.*, **40**, 1185–1206.
- Seifert, A. K., 2005: On the shape–slope relation of drop size distributions in convective rain. *J. Appl. Meteor.*, **44**, 1146–1151.
- , and D. Beheng, 2001: A double-moment parameterization for simulating autoconversion, accretion and self-collection. *Atmos. Res.*, **59–60**, 265–281.
- Smith, P. L., C. G. Myers, and H. D. Orville, 1975: Radar reflectivity factor calculations in numerical cloud models using bulk parameterization of precipitation. *J. Appl. Meteor.*, **14**, 1156–1165.
- , Z. Liu, and J. Joss, 1993: A study of sampling-variability effects in raindrop size observations. *J. Appl. Meteor.*, **32**, 1259–1269.
- Steiner, M., J. A. Smith, and R. Uijlenhoet, 2004: A microphysical interpretation of radar reflectivity–rain rate relationships. *J. Atmos. Sci.*, **61**, 1114–1131.
- Sun, J., 2005: Initialization and numerical forecasting of a supercell storm observed during STEPS. *Mon. Wea. Rev.*, **133**, 793–813.
- , and N. A. Crook, 1997: Dynamical and microphysical retrieval from Doppler radar observations using a cloud model and its adjoint. Part I: Model development and simulated data experiments. *J. Atmos. Sci.*, **54**, 1642–1661.
- , and —, 1998: Dynamical and microphysical retrieval from Doppler radar observations using a cloud model and its adjoint. Part II: Retrieval experiments of an observed Florida convective storm. *J. Atmos. Sci.*, **55**, 835–852.
- , and —, 2001: Real-time low-level wind and temperature analysis using single WSR-88D data. *Wea. Forecasting*, **16**, 117–132.
- Thompson, G., R. M. Rasmussen, and K. Manning, 2004: Explicit forecasts of winter precipitation using an improved bulk microphysics scheme. Part I: Description and sensitivity analysis. *Mon. Wea. Rev.*, **132**, 519–542.
- Ulbrich, C. W., 1983: Natural variations in the analytical form of the raindrop size distribution. *J. Climate Appl. Meteor.*, **22**, 1764–1775.
- Vivekanandan, J., G. Zhang, and E. Brandes, 2004: Polarimetric radar rain estimators based on a constrained gamma drop size distribution model. *J. Appl. Meteor.*, **43**, 217–230.
- Walko, R. L., W. R. Cotton, M. P. Meyers, and J. Y. Harrington, 1995: New RAMS cloud microphysics parameterization, Part I: The single-moment scheme. *Atmos. Res.*, **38**, 29–62.
- Warner, T., E. A. Brandes, J. Sun, D. N. Yates, and C. K. Mueller, 2000: Prediction of a flash flood in complex terrain. Part I: A comparison of rainfall estimates from radar, and very short range rainfall simulations from a dynamic model and an automated algorithmic system. *J. Appl. Meteor.*, **39**, 797–814.
- Willis, P., 1984: Function fits to some observed drop size distributions and parameterization of rain. *J. Atmos. Sci.*, **41**, 1648–1661.
- Wilson, J. W., and E. A. Brandes, 1979: A radar measurement of rainfall—A summary. *Bull. Amer. Meteor. Soc.*, **60**, 1048–1058.
- Wu, B., J. Verlinde, and J. Sun, 2000: Dynamical and microphysical retrievals from Doppler radar observations of a deep convective cloud. *J. Atmos. Sci.*, **57**, 262–283.
- Yuter, S. E., and R. A. Houze Jr., 1995: Three-dimensional kinematic and microphysical evolution of Florida cumulonimbus. Part II: Frequency distribution of vertical velocity, reflectivity, and differential reflectivity. *Mon. Wea. Rev.*, **123**, 1941–1963.
- Zhang, G., J. Vivekanandan, and E. Brandes, 2001: A method for estimating rain rate and drop size distribution from polarimetric radar measurements. *IEEE Trans. Geosci. Remote Sens.*, **39**, 830–841.
- , —, —, R. Meneghini, and T. Kozu, 2003: The shape–slope relation in observed gamma drop size distributions: Statistical error or useful information? *J. Atmos. Oceanic Technol.*, **20**, 1106–1119.
- Zhao, Q. Y., and F. H. Carr, 1997: A prognostic cloud scheme for operational NWP models. *Mon. Wea. Rev.*, **125**, 1931–1953.